Journal of Solid State Chemistry 183 (2010) 277–284

Contents lists available at ScienceDirect

Journal of Solid State Chemistry

journal homepage: www.elsevier.com/locate/jssc

Synthesis of morphology-controllable mesoporous Co_3O_4 and CeO_2

Yangang Wang, Yanqin Wang *, Jiawen Ren, Yan Mi, Fengyuan Zhang, Changlin Li, Xiaohui Liu, Yun Guo, Yanglong Guo, Guanzhong Lu *

Lab for Advanced Materials, Research Institute of Industrial Catalysis, East China University of Science and Technology, Meilong Road 130, Shanghai 200237, P.R. China

ARTICLE INFO

Article history:
Received 19 June 2009
Received in revised form
30 August 2009
Accepted 8 November 2009
Available online 11 December 2009

Keywords:
Morphology control
Mesoporous metal oxides
Nanocasting

ABSTRACT

Recently, extensive works have been devoted to the morphology control of mesoporous materials with respect to their use in various applications. In this paper, we used two kinds of mesoporous silica, SBA-15 rods and spheres as hard templates to synthesize morphology-controllable mesoporous metal oxides. By carefully controlling the loading of metal precursors in the mesopores of the hard template, mesoporous Co_3O_4 and CeO_2 with different morphologies, such as micrometer-sized rod, hollow sphere, saucer-like sphere, and solid sphere were conveniently obtained. The structural properties of these materials were characterized by XRD, BET, SEM and TEM. In addition, it is found that the differences observed in the textural properties of the two mesoporous metal oxides nanocasted from the same template can be attributed to the properties of metal precursors and the interaction between metal oxide and SiO_2. Thus-obtained mesoporous metal oxides with such special morphologies may have a potential application in the field of environmental catalytic oxidation.

1. Introduction

In recent years, the design and synthesis of mesoporous metal oxides with high thermal stability, high surface area, and crystalline framework have attracted considerable interests because of their potential applications in areas including catalysis, sorption, chemical and biological separation, photonic and electronic devices, drug delivery, and gas sensing [1–5]. Generally, there are two main methods to prepare mesoporous metal oxides, the conventional one is the so-called chemical soft templating method, which employs organic surfactants to form micelles in aqueous solutions, and than allows for a lot of mesoporous metal oxides and mixed oxides to be synthesized [1,6–9]. However, many mesoporous metal oxides prepared from this method suffered from a lot of disadvantages, such as amorphous inorganic walls, poor mesoporous structure, and thermal instability during the removal of organic templates, which greatly limited their applications to catalyst and other functional nanomaterials. Another method, the nanocasting strategy, pioneered by the group of Ryoo with the preparation of ordered mesoporous carbon (CMK-type family) [10], is a very attractive alternative. In this approach, the pores and channels of mesoporous silica or carbon are infiltrated with suitable precursors and then the mixture was subjected to heat treatment at a certain temperature to convert the precursors to oxides. After the final selective removal of the inorganic templates, the shape-reversed molded structures may be obtained. Till now, various types of mesoporous metals and metal oxides [11–15] which are usually difficult to be prepared by the direct templating methods, have been successfully nanocasted from mesoporous silica or mesoporous carbon.

From the viewpoint of various practical applications of mesoporous metal oxides, the fabrication of desired morphologies is important as well as the control in composition, structure, porosity, etc. In 2003, Gao's group [16] synthesized monodispersed mesoporous spheres of metal oxides and phosphates via a two-step nanocasting route using mesoporous carbon as a template. These novel mesoporous inorganic spheres are expected to have a variety of applications in chromatography, catalysis, and nanotechnology. By a similar method, Mokaya et al. [17] have prepared hollow spheres and shells of crystalline porous metal oxides using mesoporous carbon hollow spheres as solid template. Recently, Li et al. [18] have prepared mesoporous titania spheres with unique urchin-like morphology and tunable interior structure, which exhibited a greatly enhanced photocatalytic activity in phenol degradation. However, there are still very little studies focused on the morphological control of mesoporous metal oxides, especially with ordered mesoporous structures [19,20].

Additionally, the mesoporous silicate hosts are attracting more interest as their pore sizes and macroscopic morphologies can be easily controlled, which further control the morphology of the replica frameworks. During this sacrificial solid-templating process, the pore channel system of mesoporous metal oxides is

* Corresponding author. Fax: +86 21 64253824.
E-mail addresses: wangyanqin@ecust.edu.cn (Y. Wang), gzhlu@ecust.edu.cn (G. Lu).

0022-4596/$ - see front matter © 2009 Elsevier Inc. All rights reserved.
doi:10.1016/j.jssc.2009.11.009

usually inversely replicated from the inorganic templates, and in general, the metal oxides of a particular morphology may be fabricated by controlling the morphology of the mesoporous silica. Among the wide variety of mesoporous silica, SBA-15 type have been extensively investigated due to their special textural properties such as larger pores, thicker pore wall, and additional interconnected micropores located inside the pore walls in contrast to MCM-41 silica. Moreover, it was concluded that the presence of this interconnecting porosity of SBA-15 is a prerequisite for a faithful and stable replication of the topology of the mesoporous silica hard templates. Indeed, there are only a few attempts to finely control the morphology of the mesoporous metal oxides by using mesoporous silica as templates [21]. So, the morphology which may get effected by nanocasting process also needs detailed investigation.

The transition metal oxide, Co_3O_4 is an important antiferromagnetic p-type semiconductor which has a potential use for applications in catalysis, sensors, magnetic materials, and energy storage [22–25]. And the rare-earth oxide, CeO_2 is of particular interest due to its catalytic activity and high oxygen storage and release ability and has been widely used in three-way catalysts for automobile exhaust [26], catalysts for the oxidation of different hydrocarbons [27], adsorbent for removal of organics from polluted water [28], and solid oxide fuel cells [29]. However, the basic requirement for many applications of above materials is the preparation, which is not only reproducible on the nano-scale but also with a high surface area and tailored structure and morphology [30–32].

With regard to all the above aspects, in the present work, a series of mesoporous Co_3O_4 and CeO_2 with different morphologies (rod, hollow sphere, saucer-like sphere, and solid sphere macrostructure) were prepared by using mesoporous SBA-15 rods and spheres as templates and cobalt/cerium nitrates as precursors. In this process, SBA-15 rods with about 2 μm length were synthesized by a modified Sayari's method [33] under static conditions, and SBA-15 spheres with the diameter about 5 μm were synthesized by using a modified method [34] with adding ethanol in the reaction solution. By using SBA-15 rods as the templates, combined with two-step impregnation process, highly ordered rodlike mesoporous Co_3O_4 and CeO_2 could be successfully synthesized. By using the mesoporous silica SBA-15 spheres as the templates, mesoporous hollow sphere, saucer-like sphere or/and solid sphere metal oxides (Co_3O_4 and CeO_2) were also synthesized by one-step and multi-step impregnation process, respectively.

2. Experimental section

2.1. Chemicals

Pluronic P123 (MW=5800, $EO_{20}PO_{70}EO_{20}$) was purchased from Aldrich. Cetyltrimethylammonium bromide (CTAB), tetraethoxysilane (TEOS), hydrochloric acid, sodium hydroxide, cobalt nitrate, cerium nitrate, glycerol, and ethanol were obtained from Shanghai Chemical Co. All chemicals were used as-received without further purification.

2.2. Synthesis of mesoporous silica SBA-15 rods

The SBA-15 rod templates were prepared by a modified method reported previously [33]. In a typical synthesis, 1.8 g of P123 and equal amount of glycerol were dissolved in 69 g 1.0 M HCl aqueous solution, which was stirred at 35 °C for 6–10 h to get a transparent solution. Then, 3.87 g of TEOS was added to the above solution under vigorous stirring. After stirring for 5 min, the mixture was kept in static conditions at the same temperature for 24 h, followed by aging at 100 °C for 24 h. The resultant solid products were collected by filtration, washed with water, dried, and calcined at 550 °C for 5 h in flowing air.

2.3. Synthesis of mesoporous silica SBA-15 spheres

The SBA-15 spheres were synthesized by a modified method according to Zhao's work [34]. In a typical synthesis, 2 g of P123 and 0.2 g of CTAB were dissolved in a mixture containing 15 mL ethanol, 15 g H_2O and 45 g 2 M HCl, followed by addition of 5.8 g TEOS under stirring. After continuous stirring for 1 h at room temperature, the resulting gel was transferred to a Teflon-lined autoclave, which was heated at 80 °C for 6 h, followed by further heating at 100 °C for 12 h. The autoclave was cooled to room temperature and the solid product was obtained via filtration, air-dried, and calcined at 550 °C for 5 h under static air conditions.

2.4. Synthesis of mesoporous metal oxides with different morphology by nanocasting process

The nanocasting processes were performed using a simple impregnation method which is similar to the previous work [35]. Typically, 1.0 g of template was dispersed in 6 mL of 0.9 M ethanolic solution of metal nitrate and stirred for several hours in a 25 mL beaker, then the mixture was transferred to a clean flat Petri dish (diameter: 10 cm) and the solvent was evaporated. In order to achieve higher loadings, the above dried hybrid powder was calcined at 200 °C for 6 h to decompose the nitrate species, and then the impregnation step was repeated, but the amount of precursor was reduced to 2/3 compared to the first step. The resulting samples were calcined in air at 500 °C for 4 h with a heating ramp of 1 K/min to completely decompose the inorganic precursor. Finally, the silica template was removed using a 2 M NaOH aqueous solution at room temperature and this etching process was repeated three times.

2.5. Characterization

Small-angle X-ray diffraction (SXRD) patterns were collected in θ–2θ mode using Rigaku D/MAX-2550VB/PC diffractometer (Cu$K\alpha_1$ radiation, λ=1.5406 Å), operated at 40 kV and 200 mA (scanning step: 0.02° per second). Wide-angle XRD patterns were collected in the same mode, but operated at 100 mA. Transmission electron microscope (TEM) images were obtained with TECNAI 20S-TMIN. Scanning electron microscopy (SEM) images were performed on a JEOL JSM-6360 scanning electron microscope operating at an acceleration voltage of 20–30 kV. Nitrogen sorption isotherms were measured at 77 K on a NOVA 4200e surface area and pore size analyzer. Before the measurements, the samples were outgassed at 300 °C in vacuum for 6 h. The Brumauer–Emmett–Teller (BET) method was utilized to calculate the specific surface areas. The pore size distributions were derived from the desorption branches of the isotherms using the Barrett–Joyner–Halanda (BJH) method. The total pore volume (Vp) was estimated at a relative pressure of 0.975.

3. Results

3.1. Characterization of the template, SBA-15 rods and its replicas

The mesostructured ordering of the template, SBA-15 rods was confirmed by low-angle XRD and nitrogen sorption analysis.

Low-angle XRD pattern, shown in Fig. 1 (left), exhibits three well-resolved diffraction peaks, which are characteristics of a 2D hexagonal (*p6m*) structure. The nitrogen sorption isotherm is a type IV with a clear H_1-type hysteresis loop at high relative pressure. The material has a BET surface area of 716 $m^2 g^{-1}$, a pore volume of 1.03 $cm^3 g^{-1}$and an average pore size of 6.6 nm. The morphology of the mesoporous SBA-15 is uniform straight rods with diameters of about 0.5 μm and lengths of 2.2 μm, which can be confirmed by SEM images in Fig. 2.

By employing these mesoporous SBA-15 rods as hard template combining with a two-step impregnation process, rodlike mesoporous metal oxides Co_3O_4 and CeO_2 were successfully prepared. The low-angle XRD patterns of the two samples are shown in Fig. 3a, both patterns exhibit three obvious diffractions corresponding to (100), (110) and (200) reflection, indicating thus-prepared metal oxides are exactly reverse-replica of the template and have a long-range periodic order with hexagonal symmetry, which was further confirmed by TEM analysis (Fig. 4b, d). The high-angle XRD patterns of mesoporous Co_3O_4 and CeO_2 (Fig. 3a inset) are indicative of well-crystallized inorganic frameworks.

The SEM images in Fig. 4(a, c) show that the rod morphology of the SBA-15 templates is replicated in the mesoporous metal oxides, the average length of the rodlike Co_3O_4 and CeO_2 were 1.8 and 1.5 μm, respectively, which is a little shorter than the template, SBA-15 rods. However, the diameter of both rods does not show any decrease, it is still around 0.5 μm. Both nitrogen sorption isotherms of the rodlike Co_3O_4 and CeO_2 (Fig. 3b) exhibit a typical type-IV isotherm with a small step and an H_1-type hysteretic loop at $P/P_0 \sim 0.4–0.8$, which is the characteristic of mesoporous metal oxides prepared by hard template route. The average pore size of both oxides is ca.3.8 nm, which is consistent with the wall thickness of the template SBA-15 rods. The uptake at high pressure ($P/P_0 \sim 0.8–1.0$) for CeO_2 is associated with the void spaces between the particles. The textural properties of the rodlike Co_3O_4 and CeO_2 are summarized in Table 1.

3.2. Characterization of the template, SBA-15 spheres and its replicas

Another hard template, mesoporous SBA-15 spheres were prepared by a modified method according to the previous report [34]. The low-angle XRD pattern of this template in Fig. 5(a), exhibits one relatively broad peak corresponding to (100) reflection, and another small shoulder at high-angle 2-theta region due to the overlap of weak intensity of (110) and (200) reflection, which is an indication of wormlike mesostructure that can be confirmed by TEM analysis (Fig. 6b inset). The SEM image in Fig. 6a shows that the spherical morphology of the sample was confirmed, the size of these spheres was between 3 and 7 μm and most particles are ca. 5 μm. This spherical morphology can also be evidenced by low magnification TEM analysis (Fig. 6b). The nitrogen sorption isotherm of the SBA-15 sphere is shown in Fig. 5b, the surface area and pore volume are 873.0 $m^2 g^{-1}$ and 0.933 $cm^3 g^{-1}$, respectively.

By using this mesoporous SBA-15 spheres as hard template and combined with a one-step impregnation process, a saucer-like mesoporous Co_3O_4 sphere has been successfully prepared. This saucer-like spherical morphology of the Co_3O_4 was confirmed by the SEM images in Fig. 7. In fact, these saucer-like spheres come from the core/shell structured mesoporous Co_3O_4 spheres, which were broken with the removal of the template SiO_2. The low magnification image (Fig. 7a) shows that the broken or intact core/shell spheres are the only particle morphology. At higher magnification (Fig. 7a, inset) it is possible to observe that the inter-surface of shell and the out-surface of core are relatively rough, which may be due to the fast shrinkage of Co_3O_4 along core and out-surface during calcination. The mean diameter of the hollow spheres was about 5 μm. When the nanocasting process was done by two-step impregnation and further increased the loadings of the precursor, a solid sphere structured mesoporous Co_3O_4 could be obtained. Compared with the host template, SBA-15 sphere, Co_3O_4 solid sphere was smaller and the surface was also rough, as shown in Fig. 7c. The XRD patterns of the two mesoporous Co_3O_4 spheres are shown in Fig. 8a, a weak and relatively broad peak can be seen in the low-angle 2-theta region, which is an indication of a certain mesostructural ordering. SEM images in Fig. 7b and d show uniform wormlike mesopores for two Co_3O_4. The high-angle XRD patterns (Fig. 8a inset) indicate that the cobalt oxide exists in a high crystalline form corresponding to spinel structure. The nitrogen sorption isotherms of the two samples were shown in Fig. 8b, which is a typical type-IV isotherm for mesoporous materials. Some typical textural parameters of these two samples are also summarized in Table 1.

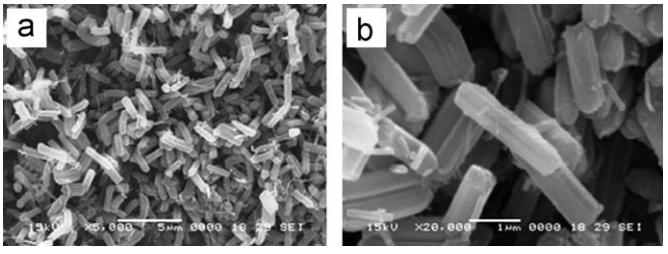

Fig. 2. Low-(a) and high-magnification (b) SEM images of mesoporous SBA-15 rods template.

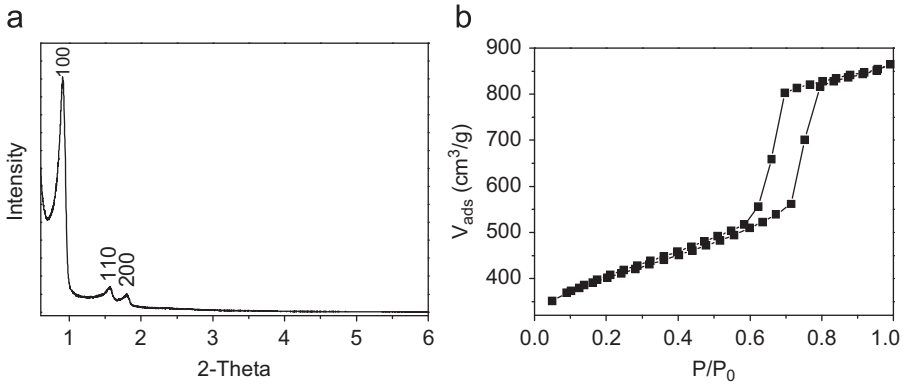

Fig. 1. (a) Low-angle XRD pattern and (b) N_2 sorption isotherms of the mesoporous SBA-15 nanorods after calcined at 550 °C for 5 h.

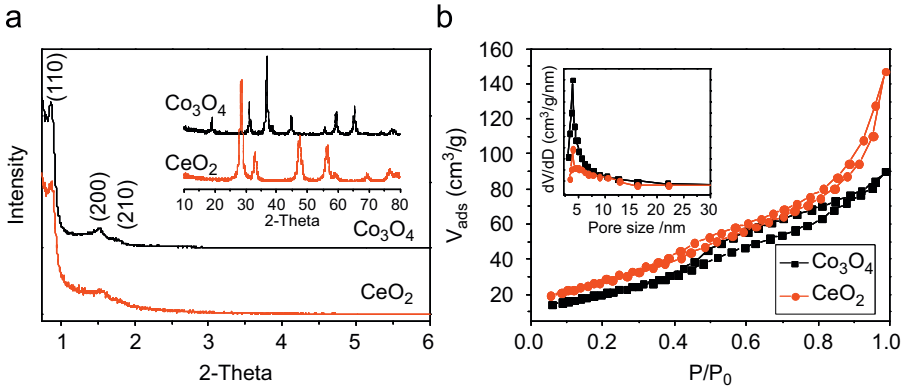

Fig. 3. (a) XRD patterns and (b) N_2 sorption isotherms and pore size distribution (insert) of the rodlike mesoporous Co_3O_4 and CeO_2.

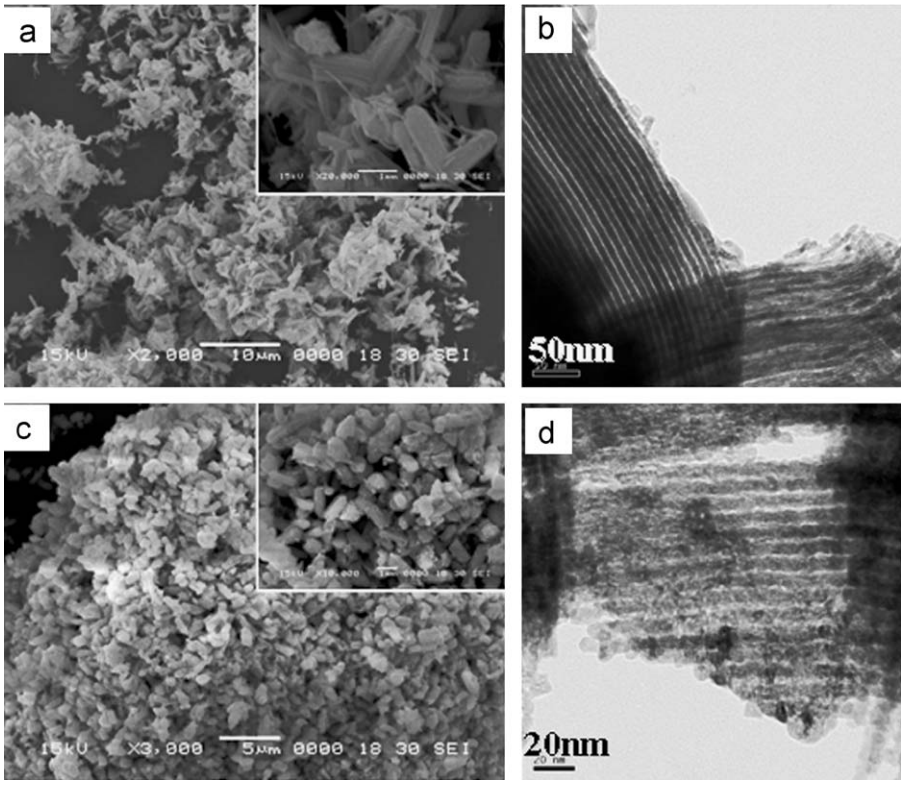

Fig. 4. SEM images of the rodlike mesoporous Co_3O_4 (a) and CeO_2 (c); TEM images of the rodlike mesoporous Co_3O_4 (b)and CeO_2 (d), respectively.

Table 1
Textural properties of various mesoporous Co_3O_4 and CeO_2 nanocasted from SBA-15 with different morphology.

Samples	Surface area/m^2 g^{-1}	Pore size/nm	Pore volume/cm^3 g^{-1}	Residual Si/wt%
Rodlike Co_3O_4	76.3	3.8	0.14	1.5
Saucer-like sphere Co_3O_4	91.8	3.7	0.15	1.5
Solid sphere Co_3O_4	94.1	3.6	0.15	1.6
Rodlike CeO_2	101.3	3.8	0.23	2.3
Hollow sphere CeO_2	161.2	3.4	0.37	2.4
Solid sphere CeO_2	164.4	3.3	0.36	2.3

Through the same process, if cerium (III) nitrate was employed as a metal precursor, the hollow spheres and solid spheres of mesoporous CeO_2 could be prepared through one-step or two-step impregnation process. Fig. 10 shows the SEM and TEM images of two samples nanocasted from the mesoporous SBA-15 spheres. As for CeO_2 hollow spheres, the images reveal the existence of both broken and relatively intact hollow spheres with relatively thick outer shells. It should be noted that the CeO_2 solid spheres prepared by two-step impregnation process well maintained the original morphology of the host template, silica, which may be due to the strong interaction between rare-earth metal elements and silica during the calcination [36]. Most

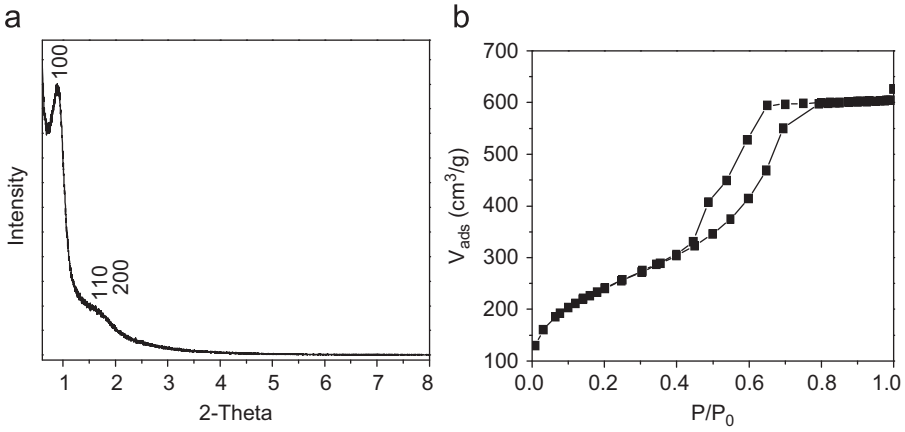

Fig. 5. (a) Low-angle XRD pattern and (b) N_2 sorption isotherms and pore size distribution (inset) of the mesoporous silica SBA-15 spheres.

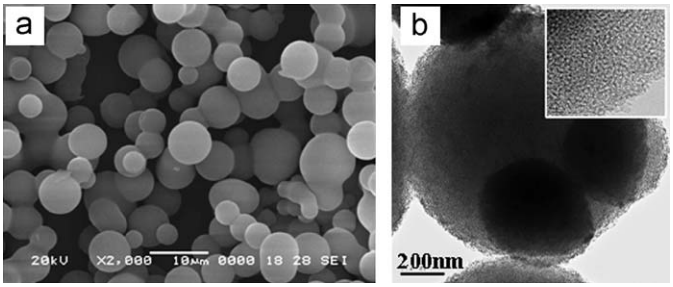

Fig. 6. SEM (a) and TEM (b) images of mesoporous silica SBA-15 spheres.

importantly, we found that the outer surface of CeO_2 spheres are smoother compared with that of Co_3O_4. The XRD patterns (Fig. 9a) of both CeO_2 spheres show a weak and relative broad peak in the low-angle 2-theta region, high-angle XRD pattern (Fig. 9a inset) indicates that the cerium oxide exists in a high crystalline form corresponding to the cubic fluorite phase. TEM images confirmed the presence of relatively ordered wormlike mesoporous. However, the nitrogen sorption isotherms of two samples shown in Fig. 9b are different from Co_3O_4 spheres. There are two hysteretic loops at $P/P_0 \sim 0.4$–0.6 and 0.7–1.0, while the first loop is assigned to mesostructure nanocasted from template, and the later is ascribed to the void spaces between the small particles. The textural properties of both CeO_2 spheres are also summarized in Table 1.

4. Discussion

From SEM images and Table 1, some differences could be found between mesoporous Co_3O_4 and CeO_2 nanocasted from the same mesoporous silica template. The surface areas and pore volume of mesoporous CeO_2 are much higher than those of mesoporous Co_3O_4, but the pore size is slightly smaller. In theory, if the mesoporous metal oxides are completely the reverse-replica of the hard template, the textural properties are mainly determined by the host template and the relative density of metal oxides. Herein, the relative density of Co_3O_4 and CeO_2 is 6.07 and 7.13 g/cm^3, respectively. In general, when mesostructured Co_3O_4 and CeO_2 are nanocasted from the same hard template, the former should have a higher surface area and pore volume compared with the later due to its lower relative density. However, this deduction is contrary to our experimental results. When using SBA-15 spheres as the template, the morphology of the obtained Co_3O_4 and CeO_2 are not completely the same, e.g. core/shell structured Co_3O_4 and hollow structured CeO_2, respectively. Moreover, EDAX analysis showed that for the mesoporous Co_3O_4, about 1.5% Si was left in the samples, while for mesoporous CeO_2, more than 2.3 wt% Si was detected.

According to previous references reported for the synthesis of various mesoporous metal oxides by hard template strategy, we can find out that in the impregnation process, the difficulty of loading metal precursor into the mesoporous channels of the hard template is different. Some metal nitrates like Co and Cr are relative easier compared with Ce and Fe [21,35,37–40], but the reason for this phenomenon has not been analyzed by researchers till now. Moreover, we find that the interactions between various metal oxides and SiO_2 also have differences, for example, Sauer et al. [36] investigated the loading of rare-earth oxides in SBA-15 and suggested that a monolayer coating of the internal surfaces of SBA-15 by rare-earth oxides were formed at low loading levels, which means there is a strong interaction of silica and rare-earth elements.

Based on the above analysis and our present results, we can propose two reasons to explain the differences of the textural properties and the morphology between mesoporous Co_3O_4 and CeO_2 nanocasted from the same SBA-15: (1) for the same concentration of ethanolic solution of cobalt nitrate and cerium nitrate, the former is easier to impregnate into the mesoporous channels than the latter, which is due to its stronger capillary force. As we know, the capillary force was determined by the following two points: one is the adhesive attraction or cohesion between solution and solid, which leads to wetting or nonwetting behavior. The other is the surface tension of the solution. In general, the higher the surface tension of solution, the lower its density and the smaller channels of the substance, the more significant the capillary force. Herein we use the same hard template and same solvent, so the capillary force was mainly determined by the surface tension and density of solution. The relative density of the metal precursors used here e.g. $Co(NO_3)_2 \cdot 6H_2O$ and $Ce(NO_3)_3 \cdot 6H_2O$ is 1.88 and 4.37 g/cm^3, respectively. So the density of the ethanolic solution of cerium nitrate is higher. Moreover, the surface tension of both ethanolic solutions we think was little affected by metal nitrate. So, here the higher capillary force for the ethanolic solution of cobalt nitrate may be due to its lower relative density, which pressed cobalt precursor penetrated SBA-15 spheres deeply. (2) Compared with transition metal oxide Co_3O_4, rare-earth metal oxide CeO_2 has a stronger interaction with SiO_2. Therefore, after the first

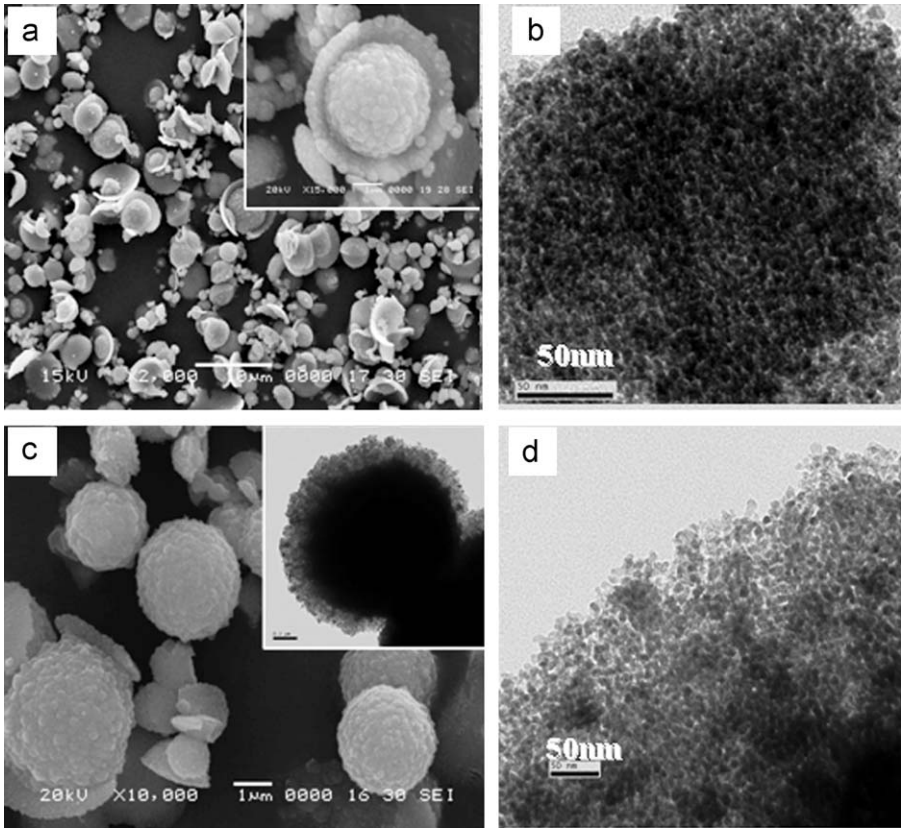

Fig. 7. SEM images of (a) the saucer-like and (c) solid sphere structure mesoporous Co_3O_4 after one and two impregnation cycles, respectively; TEM images of (b) the saucer-like and (c inset, d) solid sphere structure mesoporous Co_3O_4.

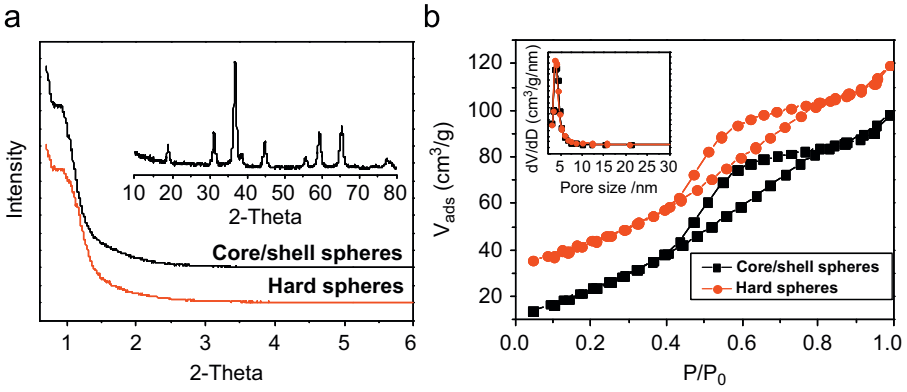

Fig. 8. (a) The XRD patterns and (b) N_2 sorption isotherms and pore size distribution (inset) of the saucer-like and solid spheres structure mesoporous Co_3O_4.

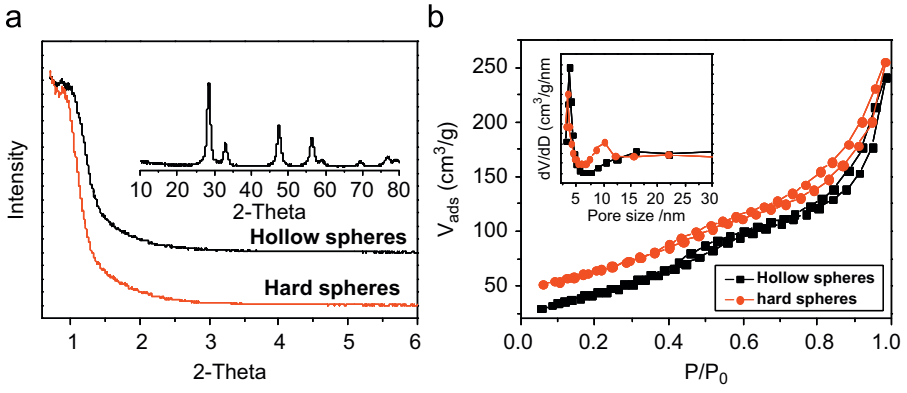

Fig. 9. (a) The XRD patterns and (b) N_2 sorption isotherms and pore size distribution (inset) of the hollow and solid sphere structure mesoporous CeO_2.

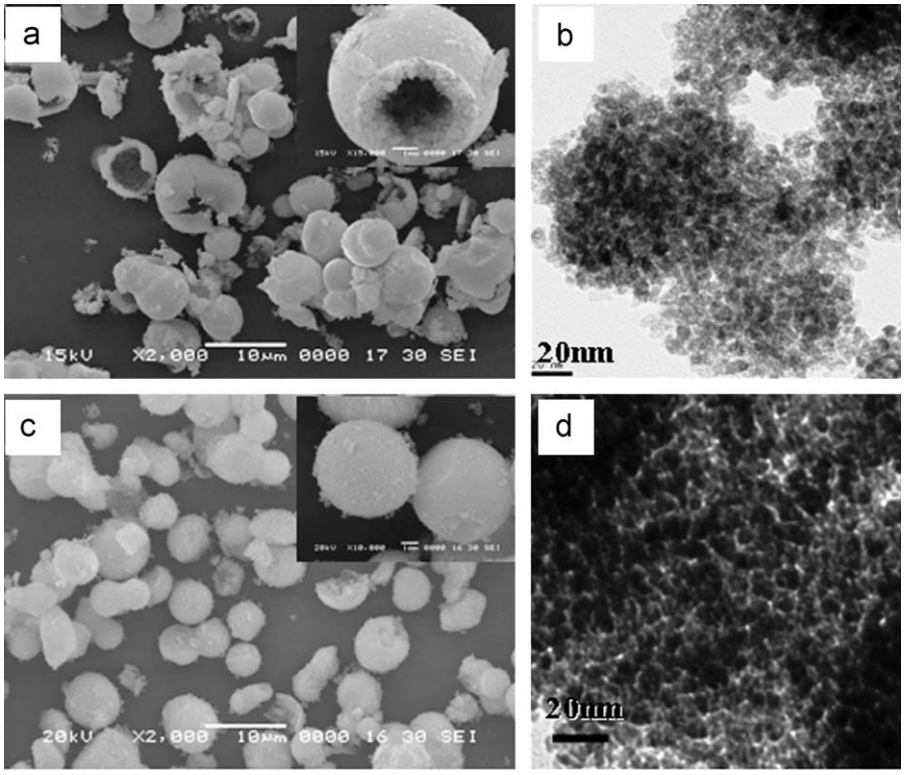

Fig. 10. SEM images of (a) the hollow and (c) solid sphere structure mesoporous CeO_2 after one and two impregnation cycles, respectively; and TEM images of (b) the hollow and (d) solid sphere structure mesoporous CeO_2.

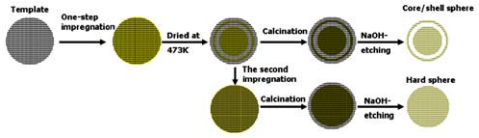

Scheme 1. Schematic illustration for the formation process of the core/shell sphere and solid sphere mesoporous Co_3O_4 by nanocasting from mesoporous SBA-15 spheres.

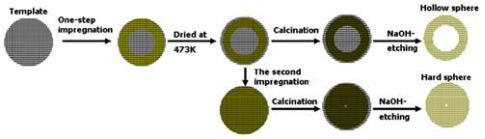

Scheme 2. Schematic illustration for the formation process of the hollow sphere and solid sphere mesoporous CeO_2 by nanocasting from mesoporous SBA-15 spheres.

impregnated sample was dried and calcined, there was a huge shrinkage along the mesopores direction for the decomposition of cobalt precursor that finally led to a core/shell structured morphology. However, cerium precursor had a little shrinkage due to the support role of SiO_2 hard template and its original form could be kept. This could also explain the different pore size between mesoporous Co_3O_4 and CeO_2. When we further increased the loading of metal precursor by re-impregnation, it will leave less space after decomposing of the precursor and a solid structure could be obtained. Additionally, due to the strong interaction between CeO_2 and SiO_2, many small CeO_2 nanoparticles will be produced after we etched the silica framework with NaOH. These small nanoparticles will lead to a high surface area. This phenomenon is more evident for the mesoporous metal oxides nanocasted from wormlike mesoporous SBA-15 spheres. In addition, it was found that the degree of crystallinity of mesoporous Co_3O_4 is higher than that of mesoporous CeO_2 from high-angle XRD patterns and TEM images of them, which is another reason for the higher surface area of mesoporous CeO_2. Scheme 1 and 2 are the formation process for the core/shell sphere, hollow sphere, and solid sphere of mesoporous Co_3O_4 and CeO_2.

5. Conclusions

In conclusion, various morphologies of mesoporous Co_3O_4 and CeO_2 (such as micrometer-sized rod, hollow sphere, core/shell sphere, and solid sphere-like structure) have been prepared by a simple nanocasting method. Thus-prepared materials have a uniform mesoporous size and high surface area, which are expected to have a promising application in the field of environmental catalysis, i.e. low temperature CO oxidation. The differences observed in the textural properties of the mesoporous Co_3O_4 and CeO_2 may be due to the properties of metal precursor and the interaction between metal oxides and SiO_2. This simple prepared method can be used to synthesis other morphology-controllable mesoporous metal oxides or sulfides.

Acknowledgments

This work was supported financially by the 973 Program of China (No. 2004CB719500), NSFC of China (No. 20673037), New Century Excellent Talents in University, China (NCET-05-415) and Shanghai Government, China (08JC1407900, 05SG33).

References

[1] P. Yang, D. Zhao, D.I. Margolese, B.F. Chmelka, G.D. Stucky, et al. , Nature 396 (1998) 152.
[2] B.J. Scott, G. Wirnsberger, G.D. Stucky, et al. , Chem. Mater. 13 (2001) 3140.
[3] F. Schüth, et al. , Chem. Mater. 13 (2001) 3184.
[4] X. He, D. Antonelli, et al. , Angew. Chem. Int. Ed. 41 (2002) 214.
[5] M. Tiemann, et al. , Chem. Eur. J. 13 (2007) 8376.
[6] A.K. Sinha, K. Suzuki, et al. , Angew. Chem. Int. Ed. 44 (2005) 271.
[7] T. Katou, D. Lu, J.N. Kondo, K. Domen, et al. , J. Mater. Chem. 12 (2002) 1480.
[8] Q. Yuan, Q. Liu, W.G. Song, W. Feng, W.L. Pu, L.D. Sun, Y.W. Zhang, C.H. Yan, et al. , J. Am. Chem. Soc. 129 (2007) 6698.
[9] Z. Bian, J. Zhu, S. Wang, Y. Cao, X. Qian, H. Li, et al. , J. Phys. Chem. C 112 (2008) 6258.
[10] R. Ryoo, S.H. Joo, S. Jun, et al. , J. Phys. Chem. B 103 (1999) 7743.
[11] H.F. Yang, D.Y. Zhao, et al. , J. Mater. Chem. 15 (2005) 1217.
[12] A.H. Lu, F. Schüth, et al. , Adv. Mater. 18 (2006) 1793.
[13] C. Dickinson, W.Z. Zhou, R.P. Hodgkins, Y.F. Shi, D.Y. Zhao, H.Y. He, et al. , Chem. Mater. 18 (2008) 3088.
[14] M. Tiemann, et al. , Chem. Mater. 20 (2008) 961.
[15] M.B. Zheng, J. Cao, S.T. Liao, J.S. Liu, H.Q. Chen, Y. Zhao, W.J. Dai, G.B. Ji, J.M. Cao, J. Tao, et al. , J. Phys. Chem. C 113 (2009) 3887.
[16] A. Dong, N. Ren, Y. Tang, Y. Wang, Y. Zhang, W. Hua, Z. Gao, et al. , J. Am. Chem. Soc. 125 (2003) 4976.
[17] Y. Xia, R. Mokaya, et al. , J. Mater. Chem. 15 (2005) 3126.
[18] H. Li, Z. Bian, D. Zhang, G. Li, Y. Huo, H. Li, Y. Lu, et al. , J. Am. Chem. Soc. 129 (2007) 4538.
[19] J. Chen, C. Burger, C.V. Krishnan, B. Chu, et al. , J. Am. Chem. Soc. 127 (2005) 14140.
[20] S. Lepoutre, J.H. Smatt, C. Laberty, H. Amenitsch, D. Grosso, M. Lindén, et al. , Microporous Mesoporous Mater. 123 (2009) 185.
[21] A. Rumplecker, F. Kleitz, E.L. Salabas, F. Schüth, et al. , Chem. Mater. 13 (2006) 3184.
[22] N. Bahlawane, E.F. Rivera, K. Kohse-Hoinghaus, A. Brechling, U. Kleineberg, et al. , Appl. Catal. B 53 (2004) 245.
[23] J. Wollenstein, M. Burgmair, G. Plescher, T. Sulima, J. Hildenbrand, H. Bottner, I. Eisele, et al. , Sens. Actuators B 93 (2003) 442.
[24] P. Poizot, S. Laruelle, S. Grugeon, L. Dupont, J.M. Tarascon, et al. , Nature 407 (2000) 496.
[25] A.G. Avila, E.C. Barrera, L.A. Huerta, S. Muhl, et al. , Sol. Energy Mater. Sol. Cells 82 (2004) 269.
[26] A. Trovarelli, et al. , Catal. Rev. Sci. Eng. 38 (1996) 439.
[27] H.C. Yao, Y.F.Y. Yao, et al. , J. Catal. 86 (1984) 254.
[28] A. Trovarelli, C. de Leitenburg, M. Boaro, G. Dolcetti, et al. , Catal. Today 50 (1999) 353.
[29] S.D. Park, J.M. Vohs, J.R. Gorte, et al. , Nature 404 (2000) 265.
[30] J.H. Smatt, B. Spliethoff, J.B. Rosenholm, M. Lindén, et al. , Chem. Commun. (2004) 2188.
[31] J.H. Smatt, C. Weidenthaler, J.B. Rosenholm, M. Lindén, et al. , Chem. Mater. 18 (2006) 1443.
[32] J.H. Smatt, N. Schüwer, M. Järn, W. Lindner, M. Lindén, et al. , Microporous Mesoporous Mater. 112 (2008) 308.
[33] A. Sayari, B.-H. Han, Y. Yang, et al. , J. Am. Chem. Soc. 126 (2004) 14348.
[34] D. Zhao, J. Sun, Q. Li, G.D. Stucky, et al. , Chem. Mater. 12 (2000) 275.
[35] Y.Q. Wang, C.M. Yang, W. Schmidt, B. Spliethoff, E. Bill, F. Schüth, et al. , Adv. Mater. 17 (2005) 53.
[36] J. Sauer, F. Marlow, B. Spliethoff, F. Schüth, et al. , Chem. Mater. 14 (2002) 217.
[37] K. Jiao, B. Zhang, B. Yue, Y. Ren, S.X. Liu, S.R. Yan, C. Dickinson, W.Z. Zhou, H.Y. He, et al. , Chem. Commun. 45 (2005) 5618.
[38] B.Z. Tian, X.Y. Liu, H.F. Yang, C.Z. Yu, B. Tu, D.Y. Zhao, et al. , Adv. Mater. 15 (2003) 1370.
[39] F. Jiao, J.-C. Jumas, M. Womes, A.V. Chadwick, A. Harrison, P.G. Bruce, et al. , J. Am. Chem. Soc. 128 (2006) 12905.
[40] S. Laha, R. Ryoo, et al. , Chem. Commun. (2003) 2138.